3D Bioprinted Vascularized Tumour

Subjects: Biotechnology & Applied Microbiology

Contributor: Seokgyu Han, Sein Kim, Zhenzhong Chen, Hwa Kyoung Shin, Seo-Yeon Lee, Hyo Eun Moon, Sun Ha Paek, Sungsu Park

An in vitro screening system for anti-cancer drugs cannot exactly reflect the efficacy of drugs in vivo, without mimicking the tumour microenvironment (TME), which comprises cancer cells interacting with blood vessels and fibroblasts. Additionally, the tumour size should be controlled to obtain reliable and quantitative drug responses.

Herein, we report a bioprinting method for recapitulating the TME with a controllable spheroid size. The TME was constructed by printing a blood vessel layer consisting of fibroblasts and endothelial cells in , alginate, and fibrinogen, followed by seeding multicellular tumour spheroids (MCTSs) of glioblastoma cells (U87 MG) onto the blood vessel layer. Under MCTSs, sprouts of blood vessels were generated and surrounding MCTSs thereby increasing the spheroid size. The combined treatment involving the anti-cancer drug temozolomide (TMZ) and the angiogenic inhibitor sunitinib was more effective than TMZ alone for MCTSs surrounded by blood vessels, which indicates the feasibility of the TME for in vitro testing of drug efficacy. These results suggest that the bioprinted vascularized tumour is highly useful for understanding tumour biology, as well as for in vitro drug testing.

Keywords: Tumour microenvionemnt ; bioprinting ; blood vessel ; angiogenesis ; fibroblast

1. Introduction

In vivo tumours form a microenvironment called a tumour microenvironment (TME), where tumour cells interact with adjacent stromal cells such as endothelial cells and fibroblasts and an extracellular matrix (ECM) [1] . This interaction is closely related to cancer progression, metastasis, and drug resistance [2] . For example, tumour cells and fibroblasts secrete angiogenic factors, such as the vascular endothelial growth factor (VEGF), leading to angiogenesis, which causes peripheral endothelial cells to form new blood vessels [3][4]. In turn, new blood vessels supply tumour cells with oxygen and nutrients, which are essential for tumour progression and metastasis [5] . In addition to VEGF, fibroblasts release various inflammatory cytokines such as interleukin 6 (IL-6) and transforming growth factor β1 (TGF-β1), to induce epithelial-mesenchymal transition (EMT) by increasing the expression of N-cadherin and vimentin in tumours [6][7]. Overexpression of these proteins is associated with a poor clinical outcome in cancer patients [8]. Thus, there is an urgent need to reconstitute the TME in vitro to better understand the biological properties of tumours and accurately predict their drug responses in vivo.

Several types of cancer cells can form spheroids called multicellular tumour spheroids (MCTSs) through self-aggregation [9]. MCTSs are commonly used to mimic the TME because of their similarity to tumours in vivo. For example, MCTSs larger than 200 μm are used to mimic cancer stem cell (CSC) niche due to a hypoxic environment in their core, where the stemness of CSCs is maintained [9][10][11][12] . To accurately observe quantitative drug responses, the size of the MCTSs should be controlled in a narrow range. Various methods have been developed to achieve this goal, including concave microwells [13][14]. However, most of these MCTSs lack endothelial and stromal cells, which play an important role in aggressive behaviours of tumour cells, such as angiogenesis and invasion [15]. Recently, microfluidic devices have been developed to recapitulate TME with perfusable vascular networks that exhibit angiogenesis [16][17][18][19]. However, because microfluidic devices are difficult to mass-produce, and their liquid handling for cell culture and drug testing in the devices is relatively complicated compared to those in microwell plates, their use in high-throughput screening (HTS) of anticancer drug efficacy is limited.

Bioprinting is a method for constructing complex three-dimensional (3D) biological structures via layer-by-layer printing of a bioink that comprises an ECM and cells, according to a computer-aided design [20]. Recently, several efforts have been made to reconstitute the TME of various cancers by 3D bioprinting technologies [21], including cervical cancer [22] and triple-negative breast cancer with fibroblasts [23]. Most recently, Langer et al. [24] bioprinted a heterotypic TME that consisted of patient-derived cancer cells, fibroblasts, and endothelial cells, closely mimicking the TME in vivo. The TME is highly useful for studying the effect of stromal cells on the response of TME to drugs. However, TMEs vary in size and may not be suitable for obtaining quantitative results regarding drug efficacy.

Herein, we report a bioprinting method for constructing a vascularized TME with a controllable size to accurately determine the responses of cancer to drugs (Figure 1). The blood vessel layer was constructed by culturing bioprinted human vascular endothelial cells (HUVECs) and lung fibroblasts (LFs) in gelatine/alginate/fibrinogen (GAF) hydrogel, until it formed blood vessels with lumens. Then, MCTSs were seeded into the blood vessel layer and incubated until the endothelial cells in the blood vessel layer migrated into the MCTSs and exhibited angiogenesis while some cancer cells invaded the blood vessel layer. The biological relevance of the biofabricated TME was verified by investigating the expression of blood vessel marker CD 31, as well as the expression of vimentin and N-cadherin. The feasibility of its application for testing of drug efficacy was demonstrated by observing the differential effects of anti-cancer drugs such as temozolomide (TMZ) and sunitinib (SU) on MCTSs with and without the blood vessel layer. Since vascularized tumour can form in microwell plates using our bioprinting method, it can be used for HTS of anti-cancer drugs efficacy.

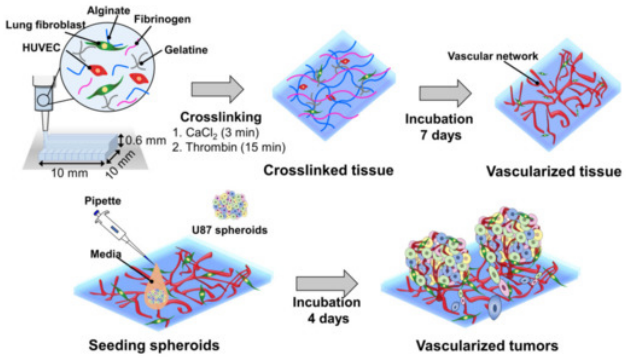

Figure 1. Combined use of bioprinted blood vessel layers and MCTSs to obtain uniform-sized vascularized tumours.

2. Microvessel Formation in GAF Hydrogel Layer Encapsulating HUVEC/LF

The ability of bioprinted hydrogel layers containing HUVECs and LFs to form blood vessels was determined by staining with DAPI for the nucleus, the anti-CD31 antibody for a blood vessel, and phalloidin for actin. On day four, the actin staining revealed capillary networks (Figure 2A) with a low expression of CD31, which is a protein expressed in endothelial intercellular junctions when endothelial cells form capillary tubes. The images showed that the capillary networks were not yet fully developed. However, on day seven, the actin staining revealed well-developed capillary networks with a high expression of CD31 (Figure 2A). This was confirmed by measuring the area and thickness of blood vessel in the layer, indicating that the blood vessels on day seven were thicker and larger than those on day four (Figures 2B and C). When the GAF hydrogel encapsulating only HUVECs was printed, microvessels were not observed until day seven, indicating that LFs are required for HUVECs to form vascularized tissues.

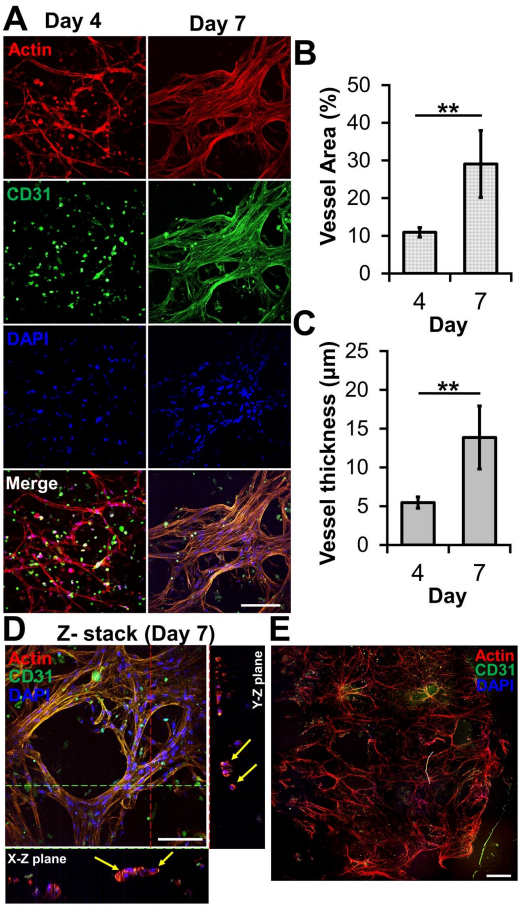

Figure 2. Microvessel formation in GAF hydrogel layer encapsulating HUVEC/LF. (A) Confocal images of microvessels in the layer stained with phalloidin (red, actin), Alexa Fluor 488-conjugated anti-CD31 antibody (green, blood vessel), and DAPI (blue, nucleus) on days four and seven. The scale bar represents 100 μm. (B) Area and (C) thickness of microvessels in the layer. Each analysis was performed by randomly selecting nine different regions in two printed layers. Student's *t*-test: $^{**}p < 0.01$. (D) Cross-sectional images of microvessels in the bioprinted layer, showing lumens. The yellow arrow indicates lumen formation. The scale bar represents 100 μm. (E) Stitched images of microvessels in the entire layer on day seven. The scale bar represents 500 μm.

3. Effects of Vascularized Tissue on Growth, Angiogenesis, and EMT of MCTSs

Compared with the MCTSs on the 3D construct without vascularized tissues (Figure 3A), those on the 3D construct with vascularized tissues exhibited more evident actin protrusions (Figure 3B) indicating that the migratory activity of cancer cells increased [25]. The 3D images indicated that neovascularized structures infiltrated into MCTSs from the vascularized tissues (Figs. 3Bi and 3Bii). Although there was no significant difference in height (Figure 3D) or aspect ratio (Figure 3E) between the two groups, the latter was about 3.8 times larger than that without the former (Figure 3F). These results indicate that the latter grew faster in the X and Y directions than the former. Taken together, blood vessels and fibroblasts in TME play important roles in the proliferation, angiogenesis, and migration of tumours [25][26].

Interestingly, the neovascularized structure seemed to be mostly disconnected as shown in Figure 3B. A similar observation was previously reported [26]. The aggressive growth of malignant cell population and their overexpression of pro-angiogenic factors can lead to the development of disorganized blood vessel networks. In disconnected vascular networks, oxygen supply is limited lead to induced micro-regional hypoxia, which is one of the key features in TME.

To determine the biological relevance of the neovascularized MCTSs, the expression of EMT markers such as N-cadherin and vimentin in MCTSs with and without vascularized structures was measured using RT-PCR [27]. Since the MCTSs with vascularized tissue contained U87, HUVECs and fibroblasts while those without vascularized tissue did not contain TME cells, we checked expression of N-cadherin and vimentin in vascularized tissue. The expressions of both N-cadherin and vimentin in the vascularized tissue were significantly lower than that in spheroids without vascularized tissue, suggesting that cancer spheroids spontaneously increase the expressions of both genes. This is not surprising because 3D spheroids are known to have higher expression of both genes than 2D cell monolayers. The expressions of both genes in MCTSs with the vascularized tissue was approximately 1.5 times higher than that in MCTSs without vascularized structures (Figure 3G). Since both genes are involved in angiogenesis and invasion of cancer cells in TME [28], the increase in the

expressions of both genes in the MCTSs seeded onto the vascularized tissue might have contributed to the formation of neovascularized structures and spiked actin structures, an indicator for cell invasion. When the neovascularized structures formed into MCTSs, some growth factors released from the neovascularized structures might have increased the expressions of both genes. Taken together, this result supports that TME were well recapitulated in the bioprinted vascularized tumour.

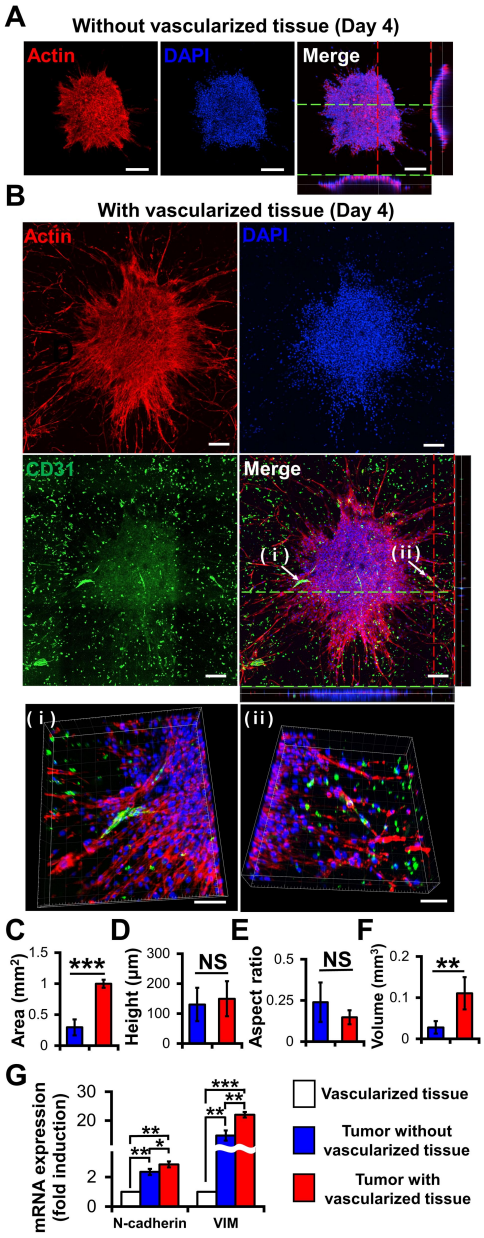

Figure 3. Effects of vascularized tissues on the growth and morphology of U87 MCTS. Confocal images of MCTSs without (**A**) and with (**B**) vascularized tissues. The scale bar represents 200 μm or (B (i, ii)) 100 μm. (**C**) Area, (**D**) height, (**E**) aspect ratio and (**F**) volume of tumours were measured for MCTSs with/without vascularized tissues. Data were obtained using 4–6 MCTSs in two tissues for each sample. Student's t-test; $^{**}p < 0.01$, $^{***}p < 0.001$; "NS" denotes "not significant". (**G**) mRNA Expressions of N-cadherin and vimentin. All experiments were performed in triplicate. Student's t-test; $^{*}p < 0.05$, $^{**}p < 0.01$, $^{***}p < 0.001$.

4. Effects of TMZ and SU on Vascularized MCTSs

To demonstrate the feasibility of the MCTSs biofabricated on the vascularized tissues for drug testing, the MCTSs were treated with the traditional anti-cancer drug TMZ, the blood vessel inhibitor SU, or with TMZ and SU together. On day zero, vascularized MCTSs were treated with TMZ and SU separately or together for three days. Actin/DAPI staining confirmed the size of the U87 MCTSs (Figure 4A). The size of MCTS was significantly reduced for the SU- and TMZ-treated samples compared with the untreated sample (Figure 4B). Additionally, there was a significant difference in size between the MCTSs treated with the different drugs. Compared with the treatments involving only TMZ or SU, those involving both TMZ and SU together further reduced the tumour size. These results are similar to the results of combination therapy involving TMZ and SU with U87 cells inserted into mice. A synergistic effect of TMZ and SU was observed when they were applied together, compared with the case where only TMZ was applied [29]. Therefore, the

results observed in this microenvironmental tissue are analogous to the in vivo results. Furthermore, because MCTSs with a uniform size were cultured at the beginning, the drug-screening results can be predicted based only on the size [30][31]. A size reduction of the MCTSs was observed in the isolinderalactone-treated samples as well (Figure S4). Isolinderalactone is an extract from *Lindera aggregata*, which is a traditional Chinese herbal medicine [32]. The result suggests that the bioprinted blood vessel layer is suitable for interaction with multiple MCTSs (approximately 4-7) and can be widely used for testing various anti-cancer drugs.

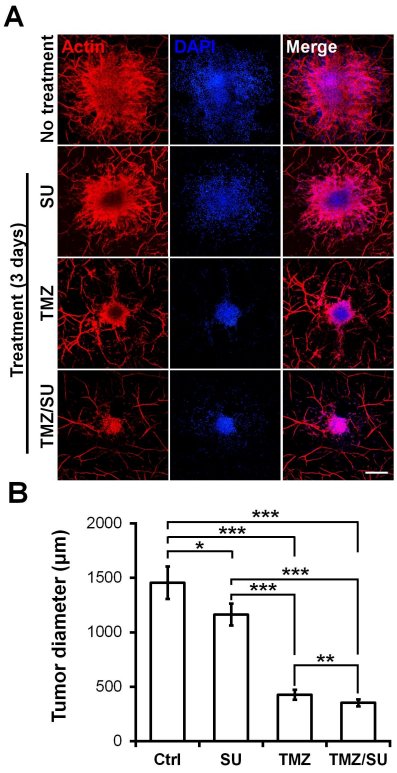

Figure 4. Synergistic effect of the anti-cancer drug TMZ and the blood vessel inhibitor SU on U87 MCTSs on vascularized tissues. (**A**) Actin (red), DAPI (blue), and merged image of MCTSs on vascularized tissue treated with TMZ (500 μM), SU (50 μM), or TMZ (500 μM)/SU (50 μM) for 72 h. The scale bar represents 500 μm. (**B**) Diameter of the drug treated MCTSs. The data were obtained for 4–6 MCTSs on two different bioprinted layers for each drug treatment. Student's t-test; *$p < 0.05$, **$p < 0.01$, ***$p < 0.001$.

References

1. Balkwill, F.R.; Capasso, M.; Hagemann, T. The Tumor Microenvironment at a Glance; The Company of Biologists Ltd: Cambridge, UK, 2012.
2. Beomseok Son; Sungmin Lee; Hyesook Youn; Eungi Kim; Wanyeon Kim; Buhyun Youn; The role of tumor microenvironment in therapeutic resistance. *Oncotarget* **2017**, *8*, 3933-3945, 10.18632/oncotarget.13907.
3. Kerbel, R.S. Tumor angiogenesis. N. Engl. J. Med. 2008, 358, 2039–2049.
4. Andrew C. Newman; Martin Nakatsu; Wayne Chou; Paul D. Gershon; Christopher Cw Hughes; The requirement for fibroblasts in angiogenesis: fibroblast-derived matrix proteins are essential for endothelial cell lumen formation. *Molecular Biology of the Cell* **2011**, *22*, 3791-3800, 10.1091/mbc.E11-05-0393.
5. Janusz W Rak; Bradley D St Croix; Robert S. Kerbel; Consequences of angiogenesis for tumor progression, metastasis and cancer therapy. *Anti-Cancer Drugs* **1995**, *6*, 3-18, 10.1097/00001813-199502000-00001.
6. Masaki Shiota; Anousheh Zardan; Ario Takeuchi; Masafumi Kumano; Eliana Beraldi; S Naito; Amina Zoubeidi; Martin Gleave4; Clusterin Mediates TGF- -Induced Epithelial-Mesenchymal Transition and Metastasis via Twist1 in Prostate Cancer Cells. *Cancer Research* **2012**, *72*, 5261-5272, 10.1158/0008-5472.can-12-0254.
7. N J Sullivan; A K Sasser; A E Axel; Farhad Vesuna; V Raman; N Ramirez; Tatiana Oberyszyn; B M Hall; Interleukin-6 induces an epithelial-mesenchymal transition phenotype in human breast cancer cells.. *Oncogene* **2009**, *28*, 2940-7, 10.1038/onc.2009.180.
8. Do-Hyun Nam; Jin-Ku Lee; Kyeung Min Joo; Jeongwu Lee; Yeup Yoon; Targeting the epithelial to mesenchymal transition in glioblastoma: the emerging role of MET signaling. *OncoTargets and Therapy* **2014**, *7*, 1933-1944, 10.2147/OTT.S36582.

9. Louis-Bastien Weiswald; Dominique Bellet; Virginie Dangles-Marie; Spherical cancer models in tumor biology.. *Neoplasia* **2015**, *17*, 1-15, 10.1016/j.neo.2014.12.004.

10. Sang-Eun Yeon; Da Yoon No; Sang-Hoon Lee; Suk Woo Nam; Il-Hoan Oh; Jaehwi Lee; Hyo-Jeong Kuh; Application of Concave Microwells to Pancreatic Tumor Spheroids Enabling Anticancer Drug Evaluation in a Clinically Relevant Drug Resistance Model. *PLOS ONE* **2013**, *8*, e73345, 10.1371/journal.pone.0073345.

11. Wanyoung Lim; Hong-Hoa Hoang; Daeun You; Jeonghun Han; Jeong Lee; Sangmin Kim; Sungsu Park; Wangyoung Lim; Jeunghum Han; Formation of size-controllable tumour spheroids using a microfluidic pillar array (μFPA) device. *The Analyst* **2018**, *143*, 5841-5848, 10.1039/c8an01752b.

12. Jeonghun Han; Seunghan Oh; Hong-Hoa Hoang; Dao Thi Thuy Nguyen; Wanyoung Lim; Tae Hwan Shin; Gwang-Hee Lee; Sungsu Park; Recapitulation of cancer stem cell niches in glioblastoma on 3D microfluidic cell culture devices under gravity-driven perfusion. *Journal of Industrial and Engineering Chemistry* **2018**, *62*, 352-361, 10.1016/j.jiec.2018.01.015.

13. Gianpiero Lazzari; Patrick Couvreur; Simona Mura; Multicellular tumor spheroids: a relevant 3D model for the in vitro preclinical investigation of polymer nanomedicines. *Polymer Chemistry* **2017**, *8*, 4947-4969, 10.1039/c7py00559h.

14. Xiaolin Cui; Yusak Hartanto; Hu Zhang; Advances in multicellular spheroids formation. *Journal of The Royal Society Interface* **2017**, *14*, 20160877, 10.1098/rsif.2016.0877.

15. Gianpiero Lazzari; Valerie Nicolas; Michiya Matsusaki; Mitsuru Akashi; P. Couvreur; Simona Mura; Multicellular spheroid based on a triple co-culture: A novel 3D model to mimic pancreatic tumor complexity. *Acta Biomaterialia* **2018**, *78*, 296-307, 10.1016/j.actbio.2018.08.008.

16. Soojung Oh; Hyunryul Ryu; Dongha Tahk; Jihoon Ko; Yoojin Chung; Hae Kwang Lee; Tae Ryong Lee; Noo Li Jeon; “Open-top” microfluidic device for in vitro three-dimensional capillary beds. *Lab on a Chip* **2017**, *17*, 3405-3414, 10.1039/C7LC00646B.

17. Minhwan Chung; Jungho Ahn; Kyungmin Son; Sudong Kim; Noo Li Jeon; Biomimetic Model of Tumor Microenvironment on Microfluidic Platform. *Advanced Healthcare Materials* **2017**, *6*, 1700196, 10.1002/adhm.201700196.

18. Venktesh Shirure; Ye Bi; Matthew B. Curtis; Andrew Lezia; Madeleine M. Goedegebuure; S. Peter Goedegebuure; Rebecca Aft; Ryan C. Fields; Steven C. George; Tumor-on-a-chip platform to investigate progression and drug sensitivity in cell lines and patient-derived organoids. *Lab on a Chip* **2018**, *18*, 3687-3702, 10.1039/c8lc00596f.

19. Yuji Nashimoto; Ryu Okada; Sanshiro Hanada; Yuichiro Arima; Koichi Nishiyama; Takashi Miura; Ryuji Yokokawa; Vascularized cancer on a chip: The effect of perfusion on growth and drug delivery of tumor spheroid.. *Biomaterials* **2019**, *229*, 119547, 10.1016/j.biomaterials.2019.119547.

20. Murphy, S.V.; Atala, A.; 3D bioprinting of tissues and organs. *Nat. Biotechnol.* **2014**, *32*, 773, .

21. Yu Shrike Zhang; Margaux Duchamp; Rahmi Oklu; Leif W. Ellisen; Robert Langer; Ali Khademhosseini; Bioprinting the Cancer Microenvironment. *ACS Biomaterials Science & Engineering* **2016**, *2*, 1710-1721, 10.1021/acsbiomaterials.6b00246.

22. Yu Zhao; Rui Yao; Liliang Ouyang; Hongxu Ding; Ting Zhang; Kaitai Zhang; Shujun Cheng; Wei Sun; Three-dimensional printing of Hela cells for cervical tumor model in vitro. *Biofabrication* **2014**, *6*, 035001, 10.1088/1758-5082/6/3/035001.

23. Tao Jiang; Jose Gil Munguia-Lopez; Salvador Flores-Torres; Joel Grant; Sanahan Vijayakumar; Antonio De Leon-Rodriguez; Joseph M. Kinsella; Directing the Self-assembly of Tumour Spheroids by Bioprinting Cellular Heterogeneous Models within Alginate/Gelatin Hydrogels. *Scientific Reports* **2017**, *7*, 4575, 10.1038/s41598-017-04691-9.

24. Ellen M. Langer; Brittany Allen-Petersen; Shelby M. King; Nicholas D. Kendsersky; Megan A. Turnidge; Genevra M. Kuziel; Rachelle Riggers; Ravi Samatham; Taylor S. Amery; Steven L. Jacques; et al. Modeling Tumor Phenotypes In Vitro with Three-Dimensional Bioprinting.. *Cell Reports* **2019**, *26*, 608-623.e6, 10.1016/j.celrep.2018.12.090.

25. Michael Olson; Erik Sahai; The actin cytoskeleton in cancer cell motility. *Clinical & Experimental Metastasis* **2008**, *26*, 273-287, 10.1007/s10585-008-9174-2.

26. Peter Carmeliet; Rakesh K. Jain; Angiogenesis in cancer and other diseases. *Nature* **2000**, *407*, 249-257, 10.1038/35025220.

27. Ying-Ying Jing; Zhipeng Han; Shanshan Zhang; Yan Liu; Lixin Wei; Epithelial-Mesenchymal Transition in tumor microenvironment. *Cell & Bioscience* **2011**, *1*, 29, 10.1186/2045-3701-1-29.

28. Andrea Morandi; Maria Letizia Taddei; Paola Chiarugi; Elisa Giannoni; Targeting the Metabolic Reprogramming That Controls Epithelial-to-Mesenchymal Transition in Aggressive Tumors. *Frontiers in Oncology* **2017**, *7*, 40, 10.3389/fonc.2

017.00040.

29. M. Czabanka; J. Bruenner; G. Parmaksiz; T. Broggini; M. Topalovic; S.H. Bayerl; G. Auf; I. Kremenetskaia; M. Nieminen; A. Jabouille; et al. Combined temozolomide and sunitinib treatment leads to better tumour control but increased vascular resistance in O6-methylguanine methyltransferase-methylated gliomas. *European Journal of Cancer* **2013**, *49*, 2243-2252, 10.1016/j.ejca.2013.02.019.
30. Xingliang Dai; Cheng Ma; Qing Lan; Tao Xu; 3D bioprinted glioma stem cells for brain tumor model and applications of drug susceptibility. *Biofabrication* **2016**, *8*, 045005, 10.1088/1758-5090/8/4/045005.
31. C. Lee; E. Abelseth; L. De La Vega; Stephanie M. Willerth; Bioprinting a novel glioblastoma tumor model using a fibrin-based bioink for drug screening. *Materials Today Chemistry* **2019**, *12*, 78-84, 10.1016/j.mtchem.2018.12.005.
32. Cheng-Hung Chuang; Li-Yu Wang; Yuen Man Wong; En-Shyh Lin; Anti-metastatic effects of isolinderalactone via the inhibition of MMP-2 and up regulation of NM23-H1 expression in human lung cancer A549 cells. *Oncology Letters* **2018**, *15*, 4690-4696, 10.3892/ol.2018.7862.
